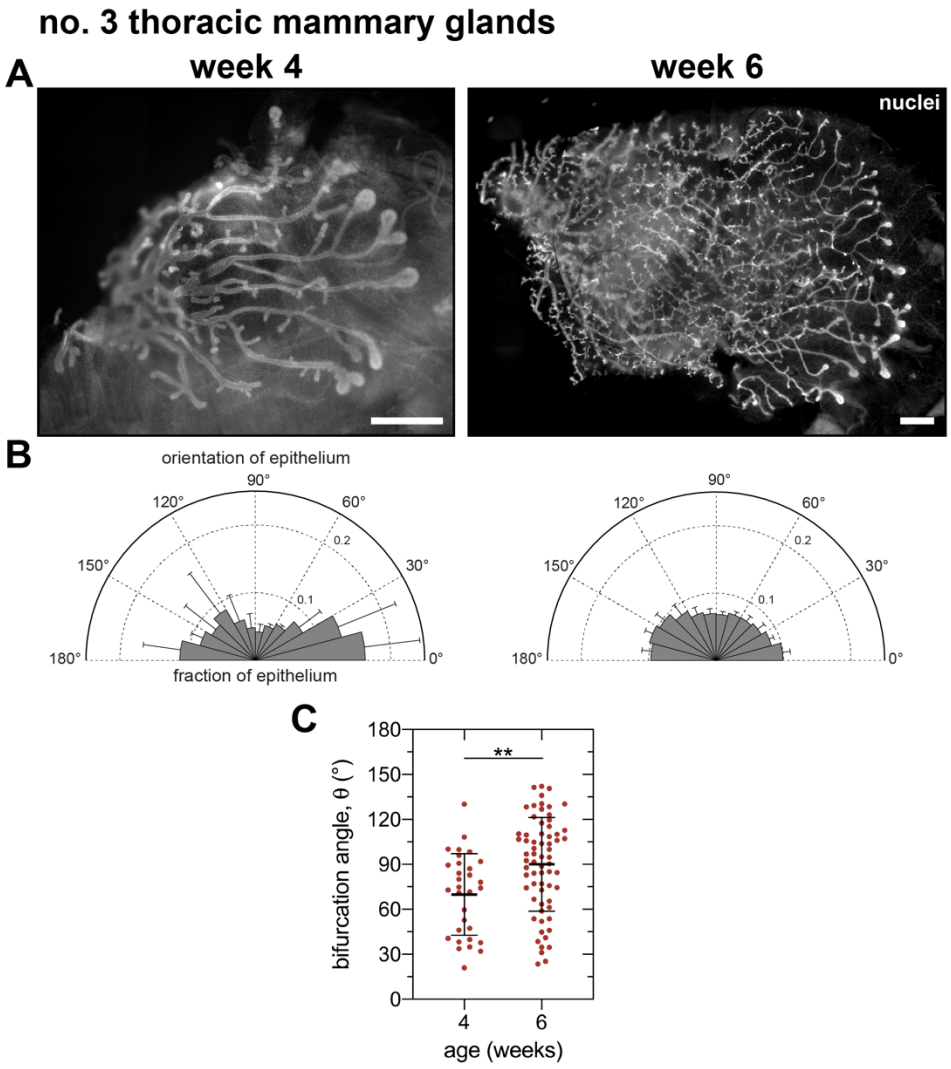

Figure S1. Epithelial orientation is biased along the long axis of pubertal thoracic mammary glands, related to Figure 1. A) Representative fluorescent images and **B**) rose plots of epithelial orientation in no. 3 thoracic mammary glands at different stages of pubertal development. Scale bars represent 1 mm. Nuclei are labeled with Hoechst 33342. **C**) Quantification of the angle of bifurcation in no. 3 thoracic mammary glands; n=31 and 67 measurements for 4- and 6-week-old glands, respectively. Data are represented as mean ± SD. $^{**}p \leq 0.01$.

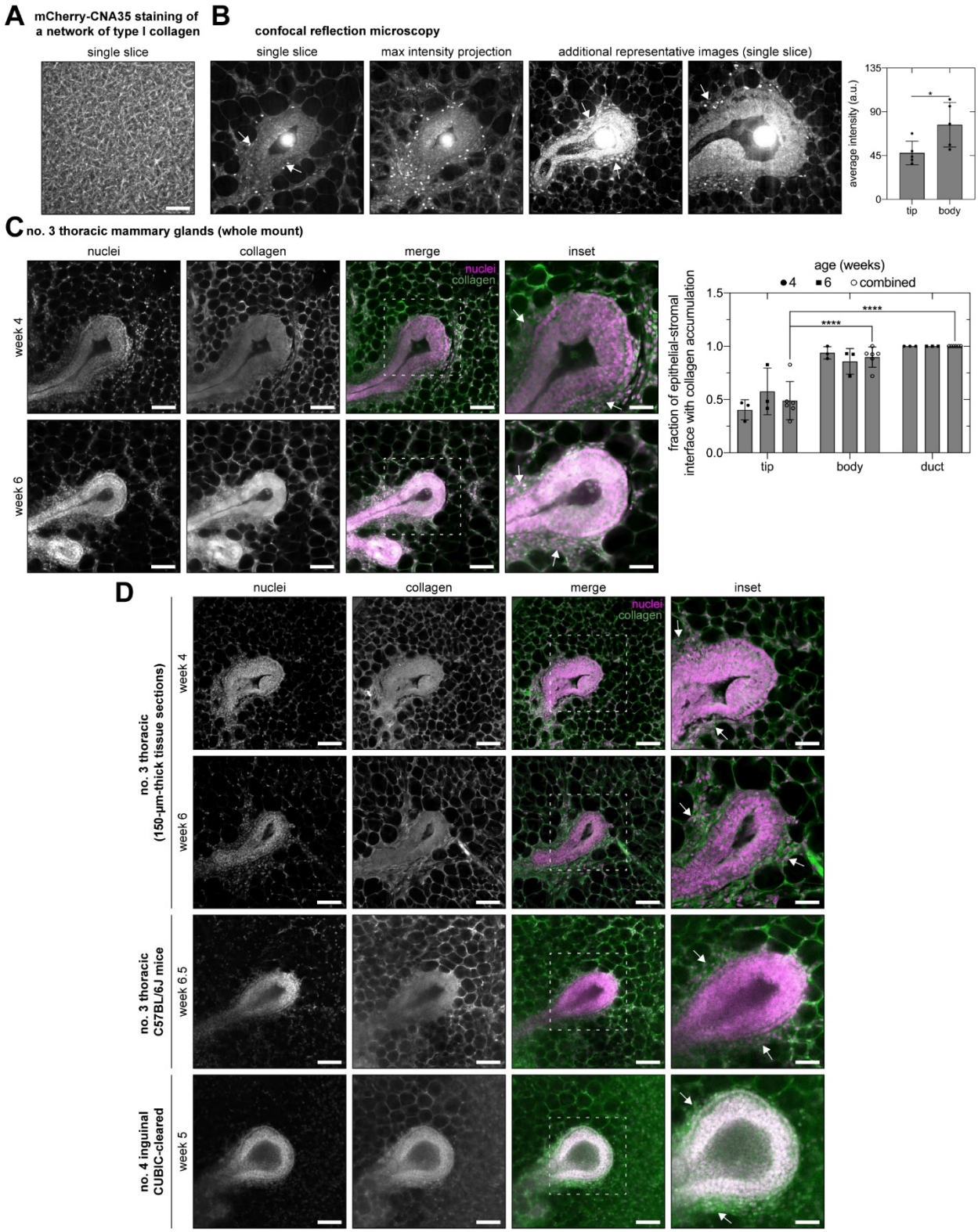
A
mCherry-CNA35 staining of a network of type I collagen
single slice
B
confocal reflection microscopy
single slice
max intensity projection
additional representative images (single slice)
average intensity (a.u.)
135
90
45
0
tip
body
C
no. 3 thoracic mammary glands (whole mount)
nuclei
collagen
merge
inset
nuclei
collagen
week 4
week 6
age (weeks)
4
6
combined
fraction of epithelial-stromal interface with collagen accumulation
1.5
1.0
0.5
0.0
****
****
tip
body
duct
D
nuclei
collagen
merge
inset
nuclei
collagen
no. 3 thoracic (150-µm-thick tissue sections)
week 4
week 6
no. 3 thoracic C57BL/6J mice
week 6.5
no. 4 inguinal CUBIC-cleared
week 5

Figure S2. TEBs extend into the fat pad in the absence of aligned networks of type I collagen at the leading edge, related to Figure 2. A) Representative fluorescent image of a network of type I collagen labeled with the collagen-binding protein mCherry-CNA35. **B**) Representative confocal reflection microscopy images of TEBs in a 4.5-week-old no. 4 inguinal mammary gland mounted in Permount and average reflection intensity at the tip and body of TEBs. **C**) Representative fluorescent confocal images of TEBs in 4- and 6-week-old no. 3 thoracic mammary glands and quantification of collagen accumulation. **D**) Representative fluorescent images of 150-μm-thick sections of TEBs in 4- and 6-week-old no. 3 thoracic glands (rows 1 and 2), TEBs in thoracic glands from C57BL/6J mice (row 3), and TEBs in 5-week-old no. 4 inguinal mammary glands cleared using CUBIC (row 4). Tissues in panels c and d are stained with Hoechst 33342 to label nuclei (magenta) and an antibody against type I collagen (green). White arrows denote collagen accumulation. Scale bars represent 100 μm or 50 μm for insets or CRM images. Data are represented as mean ± SD. ****$p \leq 0.0001$.

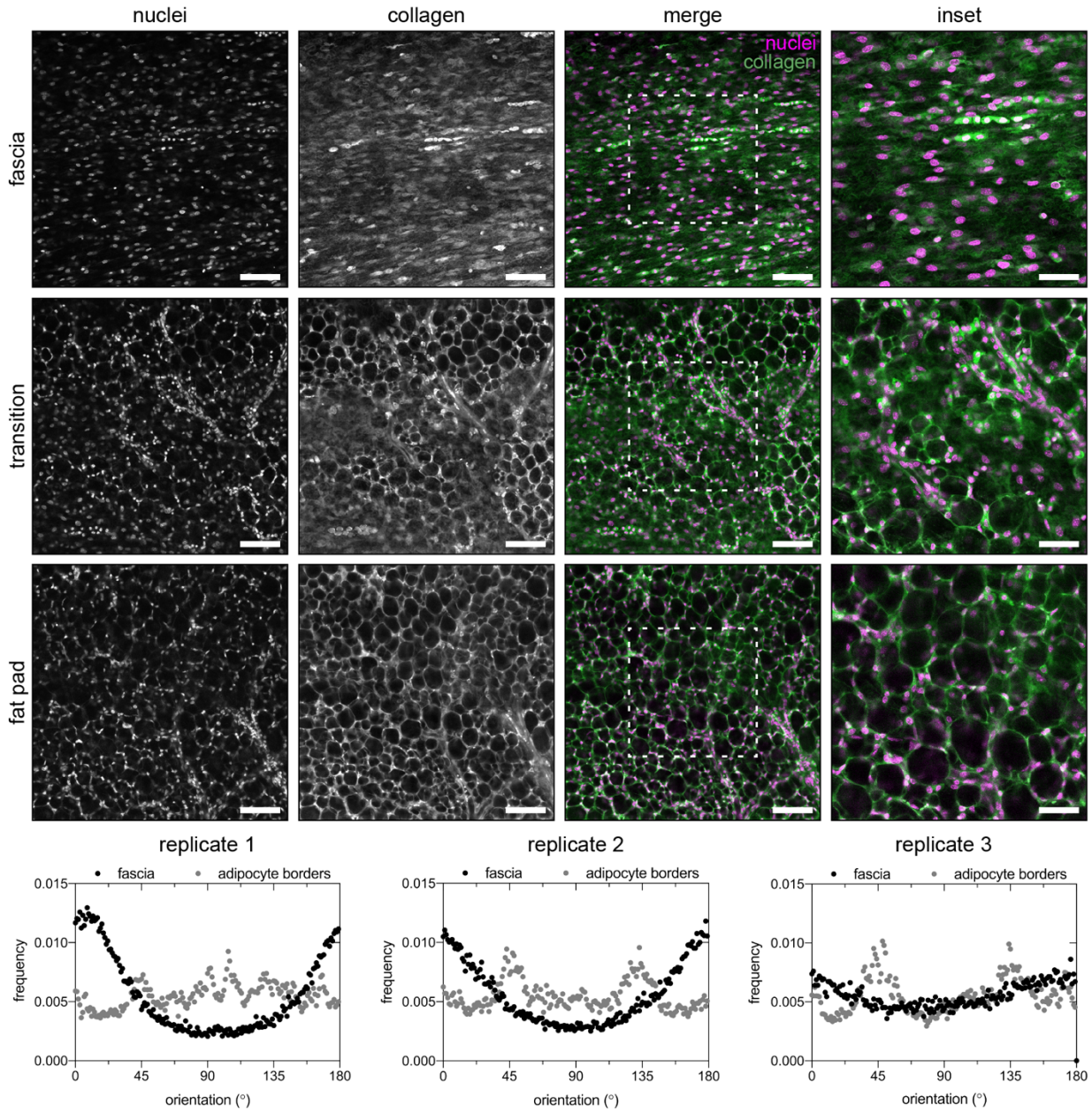

Figure S3. The network of collagen around adipocyte borders is not oriented in the same direction as collagen fibers in the adjacent fascia, related to Figure 3. Representative confocal fluorescent images of the fascia (top), transition between the fascia and the fat pad (middle), and the fat pad in a 4-week-old inguinal mammary gland (bottom). Tissues are stained with Hoechst 33342 to label nuclei (magenta) and an antibody against type I collagen (green).

Scale bars represent 100 µm or 50 µm for insets. Three representative replicates comparing the orientation of collagen fibers in the fascia with the orientation of the network of collagen around adipocytes in the adjacent fat pad.

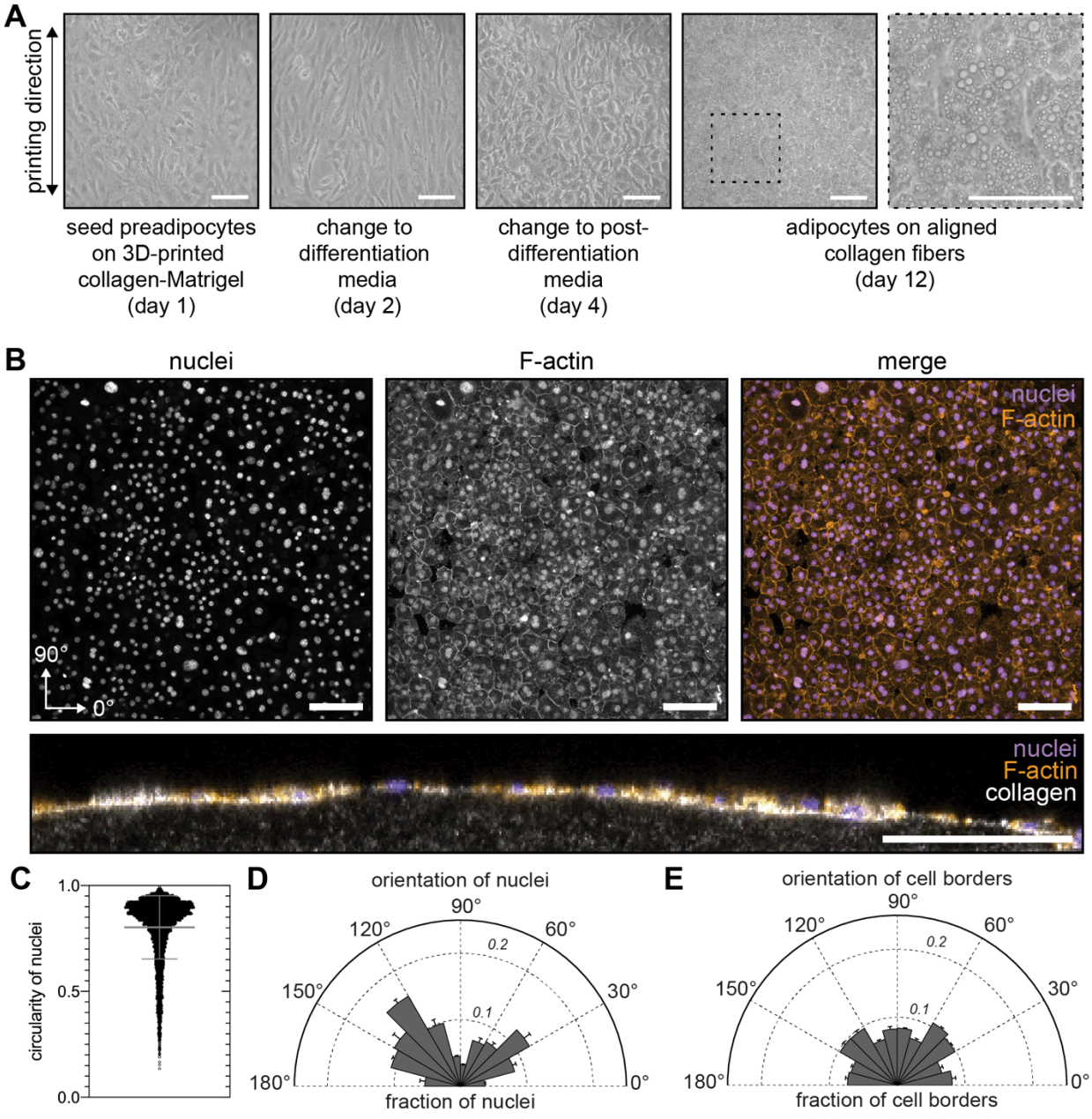

Figure S4. Adipocyte cell borders are not oriented in the same direction as collagen fibers in an adjacent 3D-printed scaffold, related to Figure 4. A) Representative phase-contrast images of 3T3-L1 cells cultured on the surface of a 3D-printed collagen-Matrigel layer throughout differentiation. Scale bars represent 100 μm. **B**) Representative confocal fluorescent images of differentiated 3T3-L1 cells on top of a 3D-printed collagen-Matrigel surface and a cross-section of a 3D-printed collagen-Matrigel line covered with a layer of adipocytes. The printing direction is oriented at 90°. Nuclei are labeled with Hoechst 33342 (blue) and F-actin is labeled with phalloidin (orange). Scale bars represent 100 μm. **C**) Circularity, **D**) orientation of cell nuclei, and **E**) orientation of cell borders for differentiated 3T3-L1 cells cultured on top of 3D-printed collagen-Matrigel. Analysis conducted for n=5397 cells. Data are represented as mean ± SD.

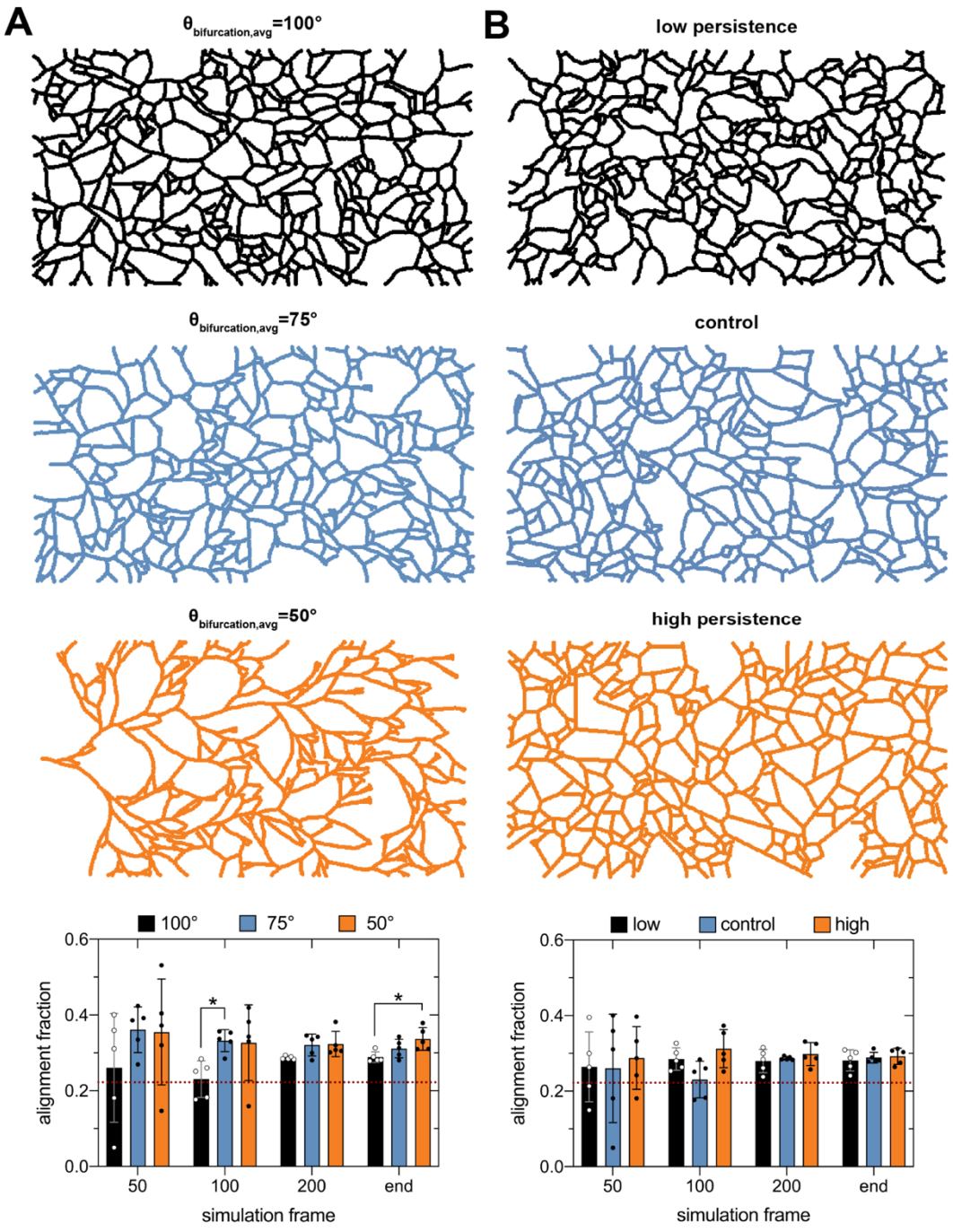

Figure S5. The angle of bifurcation of TEBs regulates both the dynamics and final magnitude of the epithelial orientation bias, related to Figure 5. Representative BARW simulations for three different **A**) average bifurcation angles and **B**) levels of persistence. Low, control, and high persistence correspond to angle diffusivity values of $\frac{\pi}{5}$, $\frac{\pi}{10}$, and 0, respectively.

The corresponding alignment fractions are shown below. Data are represented as mean ± SD. *$p \leq 0.05$.

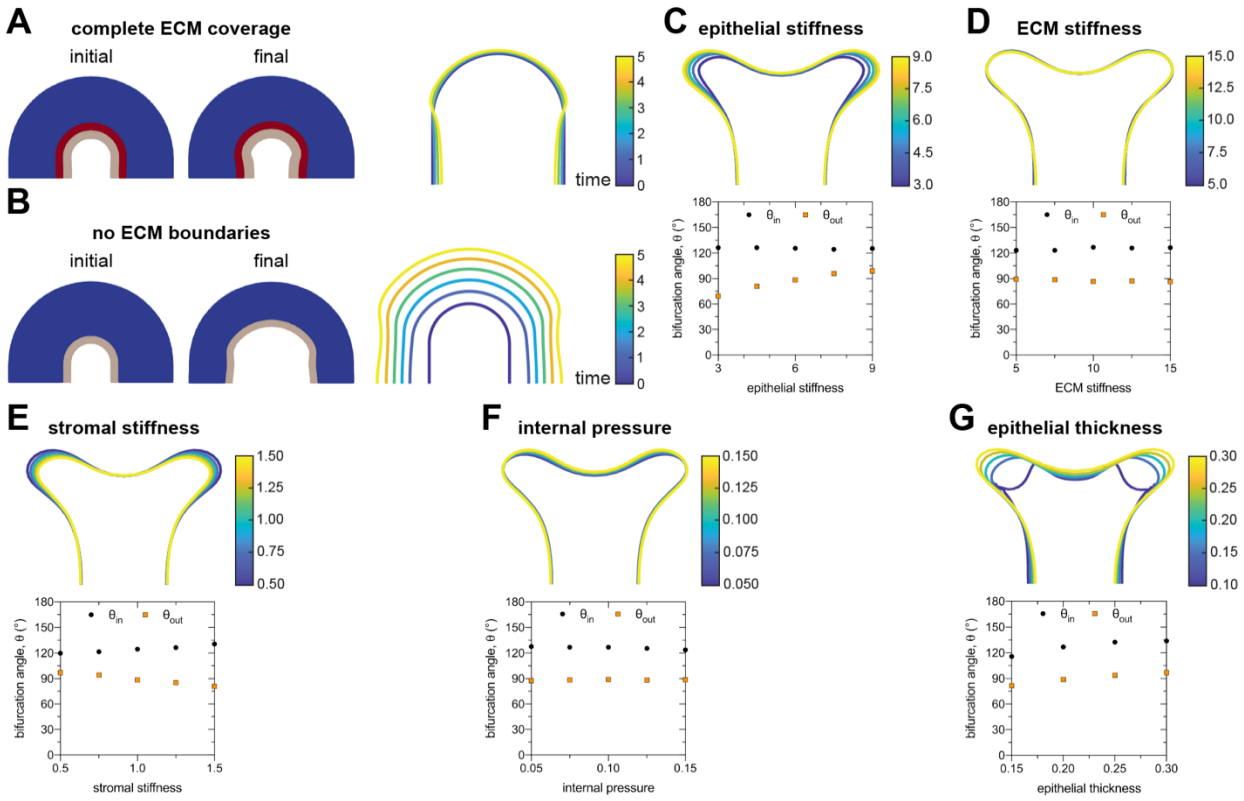

Figure S6. The mechanical properties of the local microenvironment affect the angle of bifurcation of TEBs, related to Figure 7. Schematics of initial and final time points and traces of epithelial geometry as a function of simulation time for TEBs with **A**) complete ECM coverage or **B**) no ECM coverage. Outlines of the final epithelial geometry and associated angles of bifurcation for simulations with varying **C**) epithelial stiffness, **D**) ECM stiffness, **E**) stromal stiffness, **F**) internal pressure, and **G**) epithelial thickness.